Atomic Ordering at the Liquid-Al/$MgAl_2O_4$ Interfaces from *Ab Initio* Molecular Dynamics Simulations

C. M. Fang and Z. Fan*

BCAST, Brunel University London, Uxbridge, Middlesex UB8 3PH, United Kingdom.

*Corresponding author: Tel: +44 1895 266406; FAX: +44 1895 269758;

E-mail address: Zhongyun.Fan@Brunel.ac.UK

Atomic Ordering at the Liquid-Al/$MgAl_2O_4$ Interfaces from *Ab Initio* Molecular Dynamics Simulations

C. M. Fang and Z. Fan*

BCAST, Brunel University London, Uxbridge, Middlesex UB8 3PH, United Kingdom.

*Corresponding author: Tel: +44 1895 266406; FAX: +44 1895 269758;

E-mail address: Zhongyun.Fan@Brunel.ac.UK

ABSTRACT

$MgAl_2O_4$ spinel particles exist inevitably in Al-Mg alloy melts and may act as potential substrates for heterogeneous nucleation of solid aluminum during solidification processing. In this paper we investigated systematically the atomic ordering of liquid Al adjacent to liquid-Al/$MgAl_2O_4${1 1 1} interfaces using an *ab initio* molecular dynamics simulation technique. Our simulations revealed that the interaction between the liquid metal and the spinel surface results in the formation of an ordered metal layer that terminates the substrate. This new terminating layer is positively charged, chemically bonded to the substrate, topologically rough and structurally coupled with the metal sublayers beneath the outmost oxygen layer. The present results may shed new light on the role of spinel particles in Al-Mg alloys and on heterogeneous nucleation processes in general.

Key Words: Liquid-metal/Oxide Interfaces; Ab Initio Molecular Dynamics Simulation; Heterogeneous Nucleation; Surface Roughness.

1. INTRODUCTION

$MgAl_2O_4$ spinel particles form inevitably during melting and liquid-handling of Al-Mg based alloy melts [1, 2]. The native spinel particles have an octahedral morphology with {1 1 1} facets. Moreover, $MgAl_2O_4$ particles form in steelmaking processes as Al and Mg are added to remove excess oxygen, can thus exist in the steel products as inclusions [3]. These particles have non-trivial impacts on the materials performances [1, 3, 4]. They may also act as potential nucleation sites during solidification processing [1, 5]. Recent study showed that early stage of solidification process contains several steps [6]. At temperature above the nucleation temperature, liquid metal adjacent to a solid substrate exhibits atomic ordering.

This phenomenon is referred to as prenucleation [6-8]. The epitaxial nucleation model [9] suggested that heterogeneous nucleation occurs in a layer-by-layer growth mechanism. The substrate surface provides a structural template to induce atomic ordering in the liquid, i.e., prenucleation. Prenucleation provides a precursor at the nucleation temperature for heterogeneous nucleation of the solid phase. Therefore, knowledge about prenucleation at the liquid-Al/MgA_2O_4{1 1 1} interfaces is crucial to gain insight into the role of the spinel particles in heterogeneous nucleation during solidification of Al-Mg alloys.

$MgAl_2O_4$ belongs to the spinel family with chemical formula AB_2X_4, here A, B are cations, X is an anion. Spinel has a rich variety of crystal chemistry with 56 atoms in the conventional face-centered cubic (FCC) cell with space group Fd-3m (No. 227) [10]. The structural frame consists of a distorted FCC oxygen sub-lattice (32 O atoms at the Wyckoff sites 32e) which provides 96 interstices. Al atoms occupy half of the 32 octahedral sites (16c) and Mg occupy one-eighth of the 64 tetragonal sites (8a) in $MgAl_2O_4$. Each O is coordinated by three Al and one Mg. Along its [1 1 1] axis (Fig. 1a), the structure of $MgAl_2O_4$ is composed of alternative O layers which have a two-dimensional (2D) hexagonal close-packed atomic arrangement (Figs. 1b and 1c), an Al layer (Fig. 1d) and a mixed metal layer (MgAlMg tri-sublayers) (Fig. 1g). Chemically, $MgAl_2O_4$ is an ionic compound with Mg^{2+}, Al^{3+}, and O^{2-} in the ionic model due to the large differences of electronegativity values of the metals (1.61 for Al, 1.31 for Mg in Pauling scale) and the oxygen (3.44). This implies that the smooth surfaces, e.g. the $MgAl_2O_4${1 1 1} surfaces with an O termination (Figs. 1c and 1d) contain net charges, being polar and are not stable at ambient conditions [11, 12]. However, the situation is different for polar surfaces in liquid metal as the free electrons of the metal atoms compensate the charges [13, 14]. There have been experimental and theoretical efforts to understand the structure and properties of the spinel [10], its surfaces [11, 12], metal/ceramic joints [15] and wetting of MgO single crystals by liquid Al [16].

In order to understand the early stage of solidification processes, semiempirical atomistic molecular dynamics (MD) simulations were performed to investigate atomic ordering at liquid-metal/substrate interfaces [7, 17, 18], with a substrates of lattice misfit [19] and with atomically rough substrates [20]. Parameters-free *ab initio* approaches have been applied to investigate interfaces between solid-Al and $MgAl_2O_4$ [21]. *Ab initio* molecular dynamics (AIMD) simulation technique was employed to study the atomic ordering at the liquid-Al/TiB_2{0 0 0 1} interfaces [22, 23], the chemical effects of the substrates on prenucleation at liquid-metal/solid-metal interfaces [9], and atomic ordering of liquid adjacent to the liquid-metal/oxides (MgO and α-Al_2O_3) interfaces [13, 14, 24-26]. The rich variety of the $MgAl_2O_4${1 1 1} surfaces indicates complex behaviors of prenucleation at the interfaces between liquid Al and $MgAl_2O_4${1 1 1} (hereafter denoted as L-Al/$MgAl_2O_3${1 1 1}). Here we present our AIMD simulations for the L-Al/$MgAl_2O_3${1 1 1} interfaces. The simulations reveal the formation of a metallic layer terminating the $MgAl_2O_4$ substrates. The atomic arrangements of the terminating metal layer are coupled with those at the substrate sub-surface. The obtained information is helpful for understanding the role of spinel particles in heterogeneous nucleation of Al-Mg alloys.

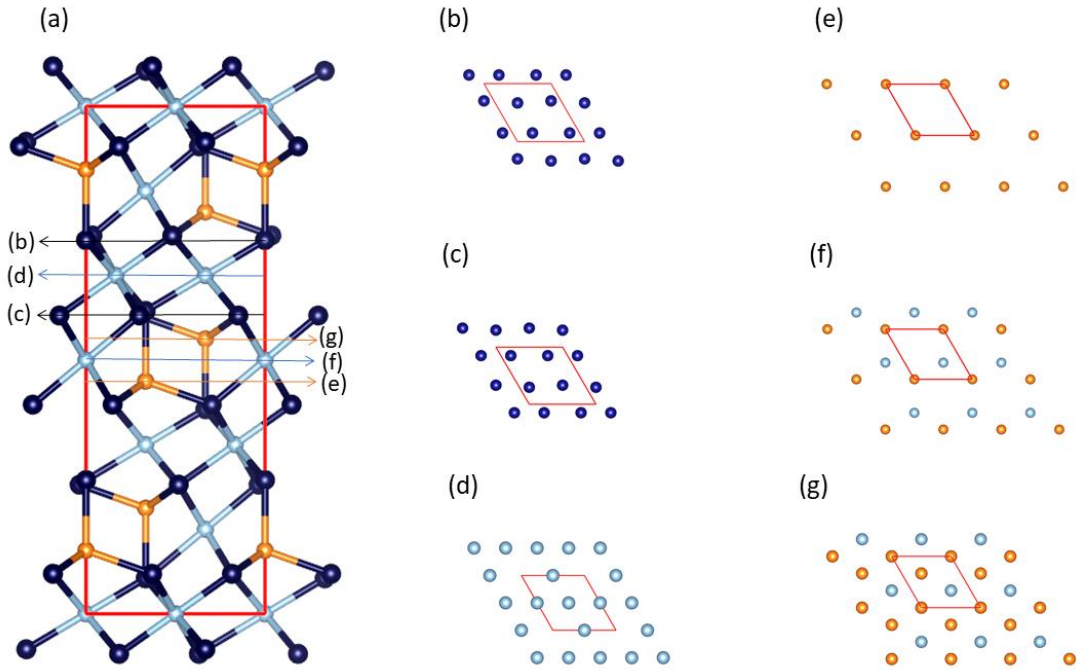

Fig.1. Schematic structure of $MgAl_2O_4$ in the hexagonal cell (a) and atomic arrangements of the related O1- (b), O2- (c), Al2- (d), Mg- sublayer (e) and MgAl- double-sublayers (f) and MgAlMg- tri-sublayers (g) terminating spinel{1 1 1}. The orange spheres represent Mg, silvery Al and dark blue O. The reddish lines represent the unit cell axis (Color figure online).

2. SIMULATION METHODS

All AIMD simulations were performed at 1000K, above the liquidus of Al. Therefore, thermal expansions of Al [27] and $MgAl_2O_4$ [28] were taken into accounts. For L-Al/$MgAl_2O_3${1 1 1}, we used $a \approx (3\sqrt{2}/2)\, a_o$, here a_o is the lattice parameter of $MgAl_2O_4$ at the simulation temperature based on the calculations and the thermal expansion. As shown in Fig. 1, there are six spinel{1 1 1} surfaces: $MgAl_2O_4\{1\,1\,1\}_{O1}$ (Fig. 1b), $MgAl_2O_4\{1\,1\,1\}_{Mg}$ (Fig. 1e), $MgAl_2O_4\{1\,1\,1\}_{MgAl}$ (Fig. 1f), $MgAl_2O_4\{1\,1\,1\}_{MgAlMg}$ (Fig. 1g), $MgAl_2O_4\{1\,1\,1\}_{O2}$ (Fig. 1b), and $MgAl_2O_4\{1\,1\,1\}_{Al2}$ (Fig. 1 d). Among them, only four are independent, considering the aggregation of liquid Al on the substrates. We designed interfaces with different substrate surfaces (Table I) based on the above analysis. Note that L-Al/$MgAl_2O_4\{1\,1\,1\}_{O2}$ and L-Al/$MgAl_2O_4\{1\,1\,1\}_{Al2}$ are among the six interfaces and will become the same at thermal equilibrium. All supercells are hexagonal with a = 17.24Å. The supercells contain four layers of oxygen atoms. The *c*-axis of the supercells were determined by the lengths of the substrate slabs and the volumes of liquid Al atoms. The supercells contain 549 to 729 atoms. Such large supercells are employed for avoiding risk of artificial crystallization of the liquid.

The simulations were performed using the first-principles' code VASP (Vienna *ab initio* simulation package), a pseudo-potential plane-wave approach within the density-functional theory (DFT) [29]. It allows variable fractional occupation numbers and therefore, works well for insulating/metallic interfaces [13, 29]. The AIMD simulation utilizes the finite-temperature density functional theory of the one-electron states, the exact energy minimization and calculation of the exact Hellmann-Feynman forces after each MD step using the preconditioned conjugate techniques, and the Nosé dynamics for generating a

canonical NVT ensemble [29]. The Gaussian smearing was employed with the width of smearing, SIGMA = 0.1eV. VASP employs the projector augmented-wave (PAW) method [30] within the generalized gradient approximation (GGA) [31]. The atomic electronic configurations in pseudo-potentials are Mg([Ne] $3s^2$ $3p^0$), Al([Ne] $3s^2$ $3p^1$) and O([He] $2s^2$ $2p^4$).

Table I. The inputs for L-Al/$MgAl_2O_4${1 1 1}$_M$, where L-Al represent liquid-Al and the subscript M represent the element at the terminating layer (Fig. 1). In the first column of the second to sixth row, the top is the input, and the bottom the equilibrated interface. All unit cells are hexagonal.

Interface	Latt. parameters(Å)	*N*(atoms)	Remarks for the inputs
L-Al/$MgAl_2O_4${1 1 1}$_{O1}$ L-Al/$MgAl_2O_4${1 1 1}$_{AlAlAl}$	*a* = 17.24, *c* = 31.51	Mg: 18; Al: 387 O: 144	O1- layer termination
L-Al/$MgAl_2O_4${1 1 1}$_{Mg}$ L-Al/$MgAl_2O_4${1 1 1}$_{MgAlAl}$	*a* = 17.24, *c* = 32.13	Mg: 36; Al: 387 O: 144	One Mg- sublayer termination
L-Al/$MgAl_2O_4${1 1 1}$_{MgAlMg}$	*a* = 17.24, *c* = 43.19	Mg: 54; Al: 531 O: 144	MgAlMg- tri-sublayers termination
L-Al/$MgAl_2O_4${1 1 1}$_{O2}$ L-Al/$MgAl_2O_4${1 1 1}$_{Al2}$	*a* = 17.24, *c* = 31.72	Mg: 36; Al: 369 O: 144	O2- layer termination
L-Al/$MgAl_2O_4${1 1 1}$_{Al1}$ L-Al/$MgAl_2O_4${1 1 1}$_{AlAlAl}$	*a* = 17.24, *c* = 42.62	Mg: 36; Al: 549 O: 144	Al1- sublayer termination

For structural optimizations, we used cut-off energies of 400.0eV for the wave functions and 550.0eV for the augmentation functions. Dense *k*-meshes were used for sampling the electronic wave functions, e.g. an 8×8×8 (35 *k*-points) in the irreducible Brillouin zone (BZ) of the conventional cell of $MgAl_2O_4$ [32]. For the AIMD simulations of the interfaces, we employed a cut-off energy of 320eV, and the Γ-point in the BZs. The dynamics of liquid/solid interfaces and molecule/solid interactions are modelled typically using Γ-point sampling due to the lack of periodicity of the overall system [22-26, 33]. Our test simulations using different cut-off energies ranging from 200.0eV to 400.0eV demonstrated that the settings are reasonable.

We prepared liquid Al samples by equilibrating at 3000K for 2000 steps (1.5fs per step), and then cooling to 1000K. We built the L-Al/$MgAl_2O_4${1 1 1} interfaces using the obtained liquid Al and the substrates. A two-step approach was employed in simulations of the interfaces. We performed AIMD simulations with the substrate O atoms pinned for about 1.5ps. Then, we equilibrated the systems with full relaxation of atoms for another 4,000 to 7,000 steps. The time-averaged method was used to sample the interfaces over 3.0ps (picosecond) to 4.5ps for attaining statistically meaningful results [13, 22-26].

3. RESULTS

The first-principles structural optimizations using the settings produced a lattice parameter of *a* = 8.086Å for cubic $MgAl_2O_4$ (experimental value 8.0812Å [27]) and 4.039Å for α-Al (experimental value 4.049Å [26]). The first-principles calculations reproduced the experimental values well.

3. 1 Atomic Layering at the L-Al/$MgAl_2O_4${1 1 1} Interfaces

We first present the atomic evolutions of the liquid adjacent to the L-Al/$MgAl_2O_4${1 1 1} interfaces. This provides us with direct impression about the formation of the interfaces. Fig. 2 displays snapshots during simulation for four independent input interfaces, L-

Al/$MgAl_2O_4\{1\ 1\ 1\}_{O1}$, L-Al/$MgAl_2O_4\{1\ 1\ 1\}_{Mg}$, L-Al/$MgAl_2O_4\{1\ 1\ 1\}_{MgAlMg}$ and L-Al/$MgAl_2O_4\{1\ 1\ 1\}_{O2}$ (Table I). At the L-Al/$MgAl_2O_4\{1\ 1\ 1\}_{O1}$ interface (Fig. 2a), the liquid atoms move quickly to the substrate, forming a new terminating Al layer of a frame of an AlAlAl tri-sublayers and therefore, we rename the equilibrated interface as L-Al/$MgAl_2O_4\{1\ 1\ 1\}_{AlAlAl}$ (Table I). The simulations showed similar evolution for another O-terminated interface, L-Al/$MgAl_2O_4\{1\ 1\ 1\}_{O2}$, which contains an Al2 layer at thermal equilibrium (Fig. 2d). The simulations also showed that at the input L-Al/$MgAl_2O_4\{1\ 1\ 1\}_{Al2}$ interface, the liquid Al move to the substrate, while some of the terminating Al atoms move towards the liquid, forming a new Al2 terminating metal layer. This newly formed Al2 layer contains vacancies (Fig. 2d) at thermal equilibrium. At L-Al/$MgAl_2O_4\{1\ 1\ 1\}_{Mg}$, the liquid Al atoms move to the interface and form a MgAlAl tri-sublayers at thermal equilibrium, as shown in Fig. 2b. At L-Al/$MgAl_2O_4\{1\ 1\ 1\}_{MgAlMg}$, the liquid Al move to the substrate, while the frame of the metal-covered substrate keeps the same (Fig. 2c). Furthermore, our simulations revealed that there is no significant difference between the input L-Al/$MgAl_2O_4\{1\ 1\ 1\}_{MgAl}$ and L-Al/$MgAl_2O_4\{1\ 1\ 1\}_{Mg}$ interfaces after about 2ps, when the systems reached their thermal equilibrium (Fig. S-1). Therefore, among the six spinel substrates, only four are independent, as shown in Fig. 2. We rename the equilibrated interfaces based on the terminating metallic (sub)layers consistently (Table I). In the rest of this paper we use the names of the equilibrated interfaces.

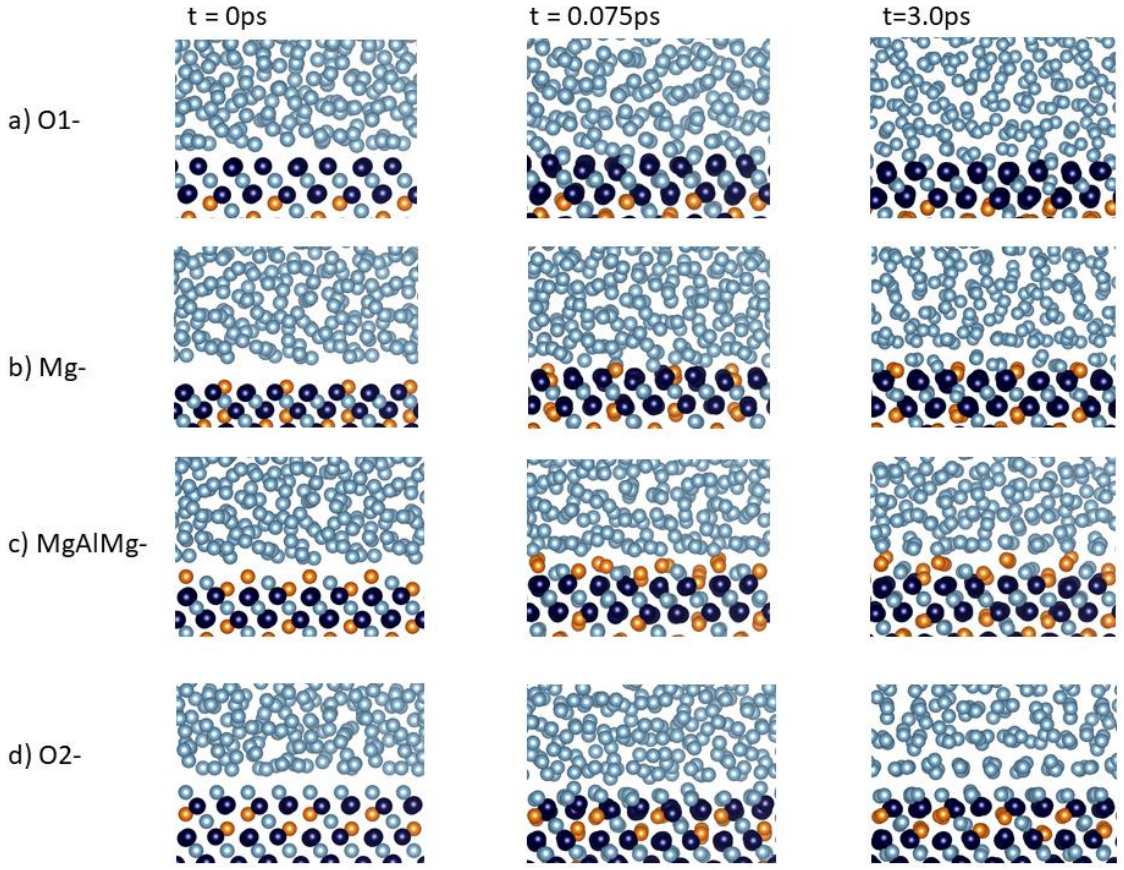

Fig. 2. Snapshots for the evolutions of the L-Al/$MgAl_2O_4\{1\ 1\ 1\}_{O1}$ (a), L-Al/$MgAl_2O_4\{1\ 1\ 1\}_{Mg}$ (b) and L-Al/$MgAl_2O_4\{1\ 1\ 1\}_{MgAlMg}$ (c) and L-Al/$MgAl_2O_4\{1\ 1\ 1\}_{O2}$ interfaces (d) (Table I) at the beginning of the *ab initio* molecular dynamics simulations (the second and third columns) and the equilibrated configurations (the last column) at 1000K. The orange spheres represent Mg, silvery Al and dark blue O (Color figure online).

We analyzed the dependences of the total valence-electron energies on simulation time for two interfaces and found that they have similar behavior. The energies decrease quickly at beginning (time < 0.5ps), and reach to the equilibrated values at about 1ps (Supplementary Materials, Fig. S-1). The simulations showed that at thermal equilibrium, the Al atoms at the terminating layer exhibit ordering and are more solid-like. However, the Al atoms adjacent to the substrates were moving around and even moved to neighboring layers. However, the numbers of Al atoms at each layer are statistically constant.

Overall, AIMD simulations revealed that the interaction between the liquid Al and the substrates causes formation of a terminating metal layer. The liquid Al atoms exhibit layering at the L-Al/$MgAl_2O_4${1 1 1} interfaces.

Atomic density profile, $\rho(z)$ provides a quantitative description of layering at a liquid/solid interface. It is defined as [7, 8, 17]:

$$\rho(z) = \langle N_z(t) \rangle / (L_x L_y \Delta z), \quad (1)$$

here, L_x and L_y are the in-plane x and y dimensions of the cell, respectively, and z the dimension perpendicular to the interface. Δz is the bin width (= 0.2Å here), and $N_z(t)$ is the number of atoms between z - (Δz/2) and z + (Δz/2) at time t. $\langle N_z(t) \rangle$ means a time-averaged number of atoms in the duration. The atomic density profiles for the L-Al/$MgAl_2O_4${1 1 1} interfaces were analyzed for the configurations summed over 3.0ps to 4.5ps (Fig. 3).

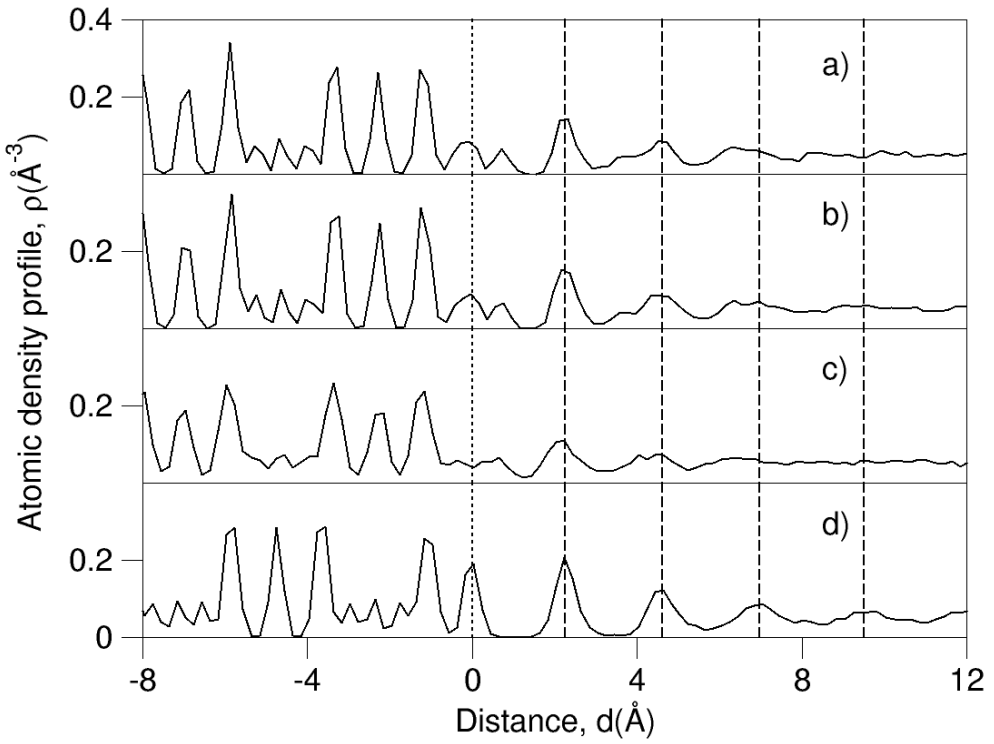

Fig. 3. Atomic density profiles at a) L-Al/$MgAl_2O_4${1 1 1}$_{MgAlMg}$, b) L-Al/$MgAl_2O_4${1 1 1}$_{MgAlAl}$, c) L-Al/$MgAl_2O_4${1 1 1}$_{AlAlAl}$, and d) L-Al/$MgAl_2O_4${1 1 1}$_{Al2}$. The dotted line (at x = 0) represents the plane of the terminating metal layer and the broken lines represent the 1st to 4th Al layer.

There are two structurally different types of terminating layers. Type 1 has three members, L-Al/$MgAl_2O_4${1 1 1}$_{AlAlAl}$, L-Al/$MgAl_2O_4${1 1 1}$_{MgAlAl}$ and L-Al/$MgAl_2O_4${1 1 1}$_{MgAlMg}$. They have a sharp Al layer beneath the outmost O-layer of the substrate, whereas Type 2 has

only one member, L-Al/$MgAl_2O_4${1 1 1}$_{Al2}$, which exhibits MgAlMg tri-sublayers at the subsurface beneath the outmost O-layer (Fig. 3).

Type 1 interfaces have broad terminating metal layers which can be recognized as three atoms sublayers (AlAlAl, MgAlAl and MgAlMg, respectively, in Figs. 2 and 3), being similar to the subsurface metal layer of the substrate of Type 2 (Fig. 1). Meanwhile, the terminating layer of Type 2 has a sharp Al peak, being similar to the subsurface Al layer of the substrate of Type 1. Therefore, the atomic arrangements of terminating metal layer at a L-Al/$MgAl_2O_4${1 1 1} interface depend on those of the metal layer at the substrate subsurface.

The prenucleation at the Type 2 interface is more pronounced than that at the Type 1 interfaces (Figs. 2 and 3). There are three clear Al peaks in the liquid Al adjacent to the L-Al/$MgAl_2O_4${1 1 1}$_{Al2}$ interface. The 1st Al layer is well separated from the terminating metal layer and the 2nd Al layer. The atoms of the 2nd Al layer are admixed with those at the 3rd Al-layer. The fourth Al layer is weak but recognizable. Meanwhile, the terminating metal layer of the Type 1 substrate is structurally similar with each other with its density peaks being broad and composed of two or three subpeaks/sublayers. There are also subtle differences among the group 1 members. The terminating metal layers containing Mg atoms have two clear subpeaks, whereas that of L-Al/$MgAl_2O_4${1 1 1}$_{AlAlAl}$ is less structured. The terminating layers of the L-Al/$MgAl_2O_4${1 1 1}$_{MgAlAl}$ and L-Al/$MgAl_2O_4${1 1 1}$_{MgAlMg}$ are well separated from the 1st Al layer, whilst the terminating Al layer at the L-Al/$MgAl_2O_4${1 1 1}$_{AlAlAl}$ is mixed with the Al atoms from the 1st Al layer.

In spite of the significant differences of their terminating Al layers, the interlayer spacing between the substrate and the 1st Al layer at all L-Al/$MgAl_2O_4${1 1 1} interface is similar. Meanwhile, the density profiles showed small spacing between the outmost O layer and the terminating metal layer, corresponding to strong interaction. Consequently, the terminating metallic atoms belong to the substrates.

3. 2 In-Plane Ordering at the L-Al/$MgAl_2O_4${1 1 1} Interfaces

The substrate surface provides a template for nucleation of the solid phase [9]. The atomic arrangements at the interface determine potency of the substrates. Fig. 4 shows snapshots for the terminating metal- and the 1st, 2nd and 3rd Al layers at the L-Al/$MgAl_2O_4${1 1 1} interfaces.

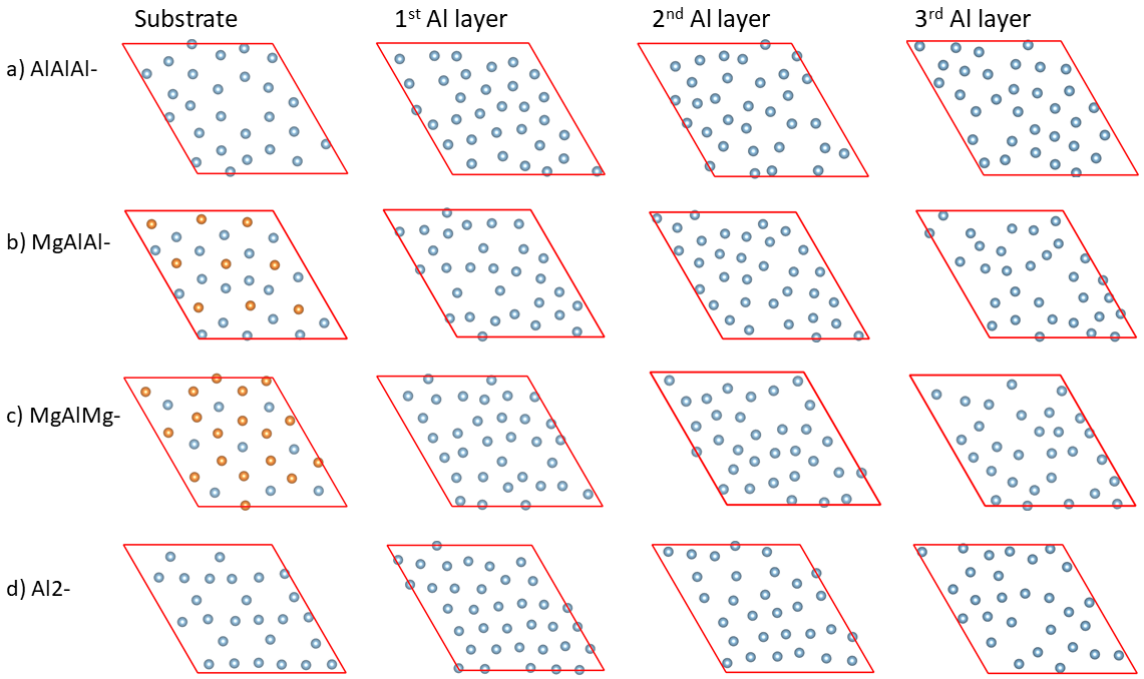

Fig. 4. Snapshots of the layer-resolved atomic arrangements at the L-Al/$MgAl_2O_4\{1\ 1\ 1\}_{AlAlAl}$ (a), L-Al/$MgAl_2O_4\{1\ 1\ 1\}_{MgAlAl}$ (b), L-Al/$MgAl_2O_4\{1\ 1\ 1\}_{MgAlMg}$ (c), and L-Al/$MgAl_2O_4\{1\ 1\ 1\}_{Al2}$ (d) interfaces. The reddish lines represent in-plane axis. The silvery spheres represent Al and the orange for Mg (Color figure online).

To quantify the atomic ordering at the interfaces, we employ in-plane ordering coefficient, $S(z)$ [7, 17]:

$$S(z) = [(\sum \exp(\boldsymbol{i}\,\boldsymbol{Q}\cdot\boldsymbol{r}_j)]^2/N_z \qquad (2)$$

where, the summation is over all atoms within a given bin of width, $\Delta z = z - (\Delta z/2)$ and $z + (\Delta z/2)$. $\boldsymbol{Q}$ is the reciprocal lattice vector, $\boldsymbol{r}_j$ is the Cartesian coordinates of the j^{th} atom, and N_z is the number of atoms in the layer. $S(z)$ assesses the atomic ordering in an individual layer. Fig. 5 shows the obtained in-plane ordering coefficients for the atomic layers near the interfaces using the configurations summed over 3ps via equation 2.

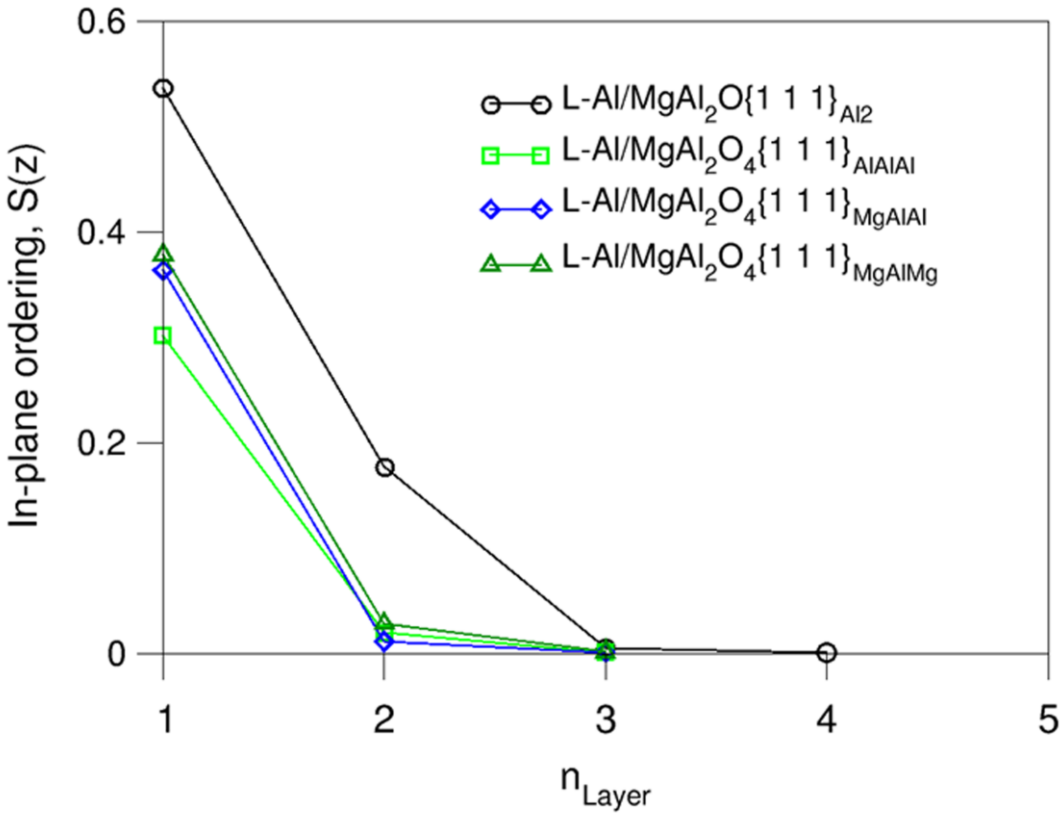

Fig. 5. In-plane ordering coefficients for the terminating Al layer (n_{Layer} = 1), the 1st Al layer (n_{Layer} = 2), and so on at the L-Al/$MgAl_2O_4${1 1 1} interfaces. (Color figure online).

At the L-Al/$MgAl_2O_4${1 1 1} interfaces the atoms at the outmost O-layer are well ordered with *S*(*z*) ~ 0.5 (not shown). Fig. 5 showed two types of interfaces which is similar to the conclusions drawn from the density profiles.

The atoms at the terminating Al-layer at L-Al/$MgAl_2O_4${1 1 1}$_{Al2}$ (Type 2) exhibit high levels of ordering with *S*(z) = 0.54. Analysis showed vacancies at the substrate (site occupation rate of 70.4%). The in-plane ordering coefficients of the rest interfaces show similar behaviors (Type 2). At L-Al/$MgAl_2O_4${1 1 1}$_{AlAlAl}$ the terminating Al atoms form a broad range (over 2Å) along the direction perpendicular to the substrate (Fig. 3). The site occupation rate is 71.8%. The substrate has the lowest in-plane ordering, *S*(z) = 0.30. The terminating metal layers adjacent to L-Al/$MgAl_2O_4${1 1 1}$_{MgAlAl}$ (*S*(z) = 0.36) and Al/$MgAl_2O_4${1 1 1}$_{MgAlMg}$ (*S*(z) = 0.38) have unusual atomic arrangements. The atoms are well-ordered in-plane but with a broad distribution (over 2Å) along *z*-axis. Analysis provided an occupation rate of 75%. The terminating layers are separated from the 1st Al layer.

The atoms at the 1st Al layer at L-Al/$MgAl_2O_4${1 1 1}$_{Al2}$ are moderately ordered with *S*(z) = 0.18, whereas the atoms at the 1st Al layer at the Type 1 interfaces are disordered (*S*(z) < 0.06), as shown in Fig. 5.

3. 3 Chemistry at the L-Al/$MgAl_2O_4${1 1 1} Interfaces

For describing the interfacial chemical interactions, we utilized Bader charge model [34]. The model provides a unique approach defining the volume and shape of an atom in a solid using the electron density distributions from quantum-mechanics calculations (Supplementary materials Fig. S-2) [34, 35]. The results for the interfaces are plotted in Fig. 6.

The charge analysis provided a clear ionic nature for the substrates with formula, $Mg^{+1.3}(Al^{+2.0})_2(O^{-1.3})_4$. The smaller charge values at the atomic sites also indicate some covalent nature of the oxide. The terminating metal atoms are charged partially, exhibiting ionic, covalent and metallic triple-nature. The charge decreases strongly with the distance from the outmost O atoms, agreeing with the bonding theory [36]. The Mg and Al atoms away from the substrates are neutral. Careful analysis revealed smaller loss of electrons for an Mg than that of an Al atom at the same position, corresponding to their valences.

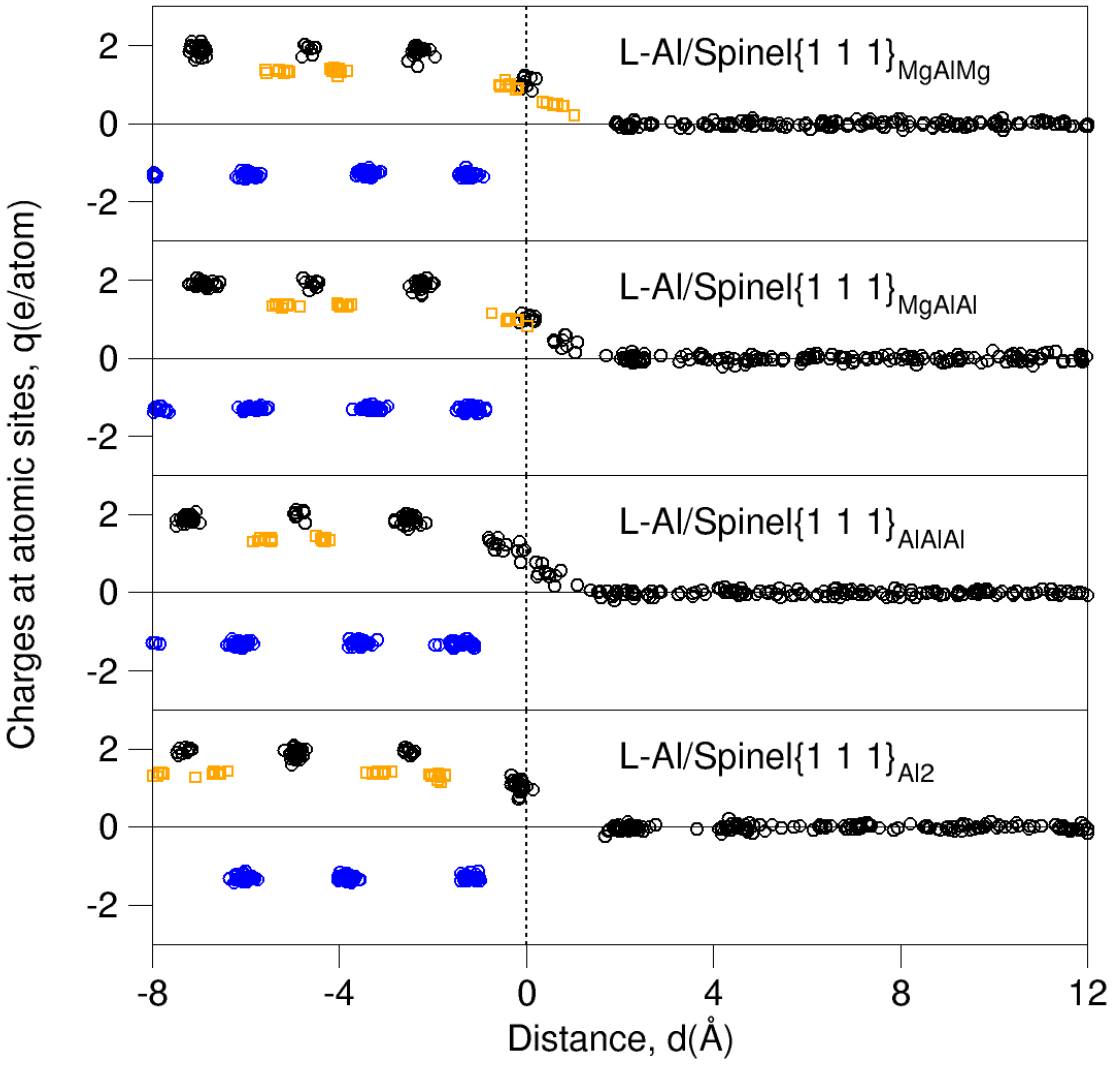

Fig. 6. Charges at the atomic sites at the L-Al/$MgAl_2O_4${1 1 1} interfaces. The black spheres represent charges at Al, orange at Mg and blue at O. (Color figure online).

3. 4 Atomic Roughness at the L-Al/$MgAl_2O_4${1 1 1} Interfaces

Atomic roughness of a layer [20] can be quantified as:

$$R = [\sum(|\Delta z(i)|/d_0)]/N_z, \quad (3)$$

where $\Delta z(i)$ is the deviation of the i^{th} atom from the atomic plane along the z-axis, $d_0(>0)$ is the interlayer spacing of the metal, and N_z is the total number of atoms in the layer. When an atom is located in the lattice of a plane, $\Delta z(i)/d_0 = 0$, when an atomic site is unoccupied, $|\Delta z(i)|/d_0 = 1.0$.

In consideration of the dynamic nature of atoms at elevated temperature, we use the density profiles for estimation of the atomic roughness. The base-plane is set to be the peak at the atomic density profile. In order to keep charge balance, the different valences of Al (3+ in ionic model) and Mg (2+) cause different N_{metal}/N_O ratio in the substrate bulk: 100.0% for MgO, 66.7% for Al_2O_3 and 75.0% for $MgAl_2O_4$. Such charge balance influences the composition and structure of the terminating metal layers at the interfaces. The triple nature of the metal atoms and high ordering at the terminating layer provide a constant free electron density at the substrate surfaces. Therefore, N_z has the same number of atoms in a substrate metal layer.

Using equation 3, we estimate R for the terminating layers at the L-Al/$MgAl_2O_4${1 1 1} interfaces. The terminating Al layer at L-Al/$MgAl_2O_4${1 1 1}$_{Al2}$ is flat with an occupation of 70.4% and therefore, has R = 6.1% with respects to difference reference. Whilst the metallic atoms at the terminating metallic layers at the rest Al/$MgAl_2O_4${1 1 1} interfaces have a complex structure (Fig. 4). We decompose the atomic density profiles according to the MgAlMg tri-sublayers in $MgAl_2O_4${1 1 1}. The splitting of the terminating atoms causes significant effective atomic roughness with R= 12.5% at L-Al/$MgAl_2O_4${1 1 1}$_{MgAlMg}$, 15.3% at L-Al/$MgAl_2O_4${1 1 1}$_{MgAlAl}$ and 19.5% at L-Al/$MgAl_2O_4${1 1 1}$_{AlAlAl}$ (Table II).

Table II. Characteristics of the oxide substrates, the terminating metal layers and related prenucleation at the selected liquid-Al/oxide interfaces (No. layers represents number of Al layers and $S(z)$ the in-plane ordering coefficient of the 1st Al layer). N_m/N_O means the atomic ration of metal to O atoms in the bulk oxides. The details of the lattice misfit, f and the atomic roughness of the metal layers are listed in the supporting materials Table S-I. *The solid atoms were pinned during the simulations [8].

Interface	f (%)	Char. M alyer N_m/N_O (%)	R(%)	q(e/M)	No. Layers	$S(z)$ 1st Al
L-Al/s-Al{1 1 1}$_{Al}$ [8]*	0	Flat. 100.0	0.0	0.00	6	0.50
L-Al/MgO{1 1 1}$_{Mg}$ [14]	-3.8	Flat 100.0	0.0	+0.69	4	0.30
L-Al/$MgAl_2O_4${1 1 1}$_{Al2}$ This work	0.2	Flat, vacancies 70.4	6.1	+1.07	4	0.18
L-Al/$MgAl_2O_4${1 1 1}$_{AlAlAl}$ This work	0.2	Vacancies, split. 71.8	19.5	+0.40 to +1.42	2 to 3	0.05
L-Al/$MgAl_2O_4${1 1 1}$_{MgAlAl}$ This work	0.2	Split 75.0	15.3	+0.33 to +1.17	3	0.02
L-Al/$MgAl_2O_4${1 1 1}$_{MgAlMg}$ This work	0.2	Split 75.0	12.5	+0.21 to +1.11	3	0.03

4. DISCUSSION

The AIMD simulations revealed that the equilibrated interfaces contain a metallic layer that terminates the $MgAl_2O_4${1 1 1} substrates. The atoms at the newly formed metal layer are strongly bonded to the outmost O atoms and exhibit ordering. Therefore, this newly formed terminating metallic layer becomes part of the substrate. The terminating metal atoms are chemically charged and structurally coupled with the substrate. The latter is schematically presented in Fig. 7. The origin of the structural coupling comes from Coulomb repulsive interaction between the metallic ions crossing the outmost O layer (see Fig. S-3). Moreover, the terminating metallic layer may contain vacancies and displacive atoms, being atomically rough.

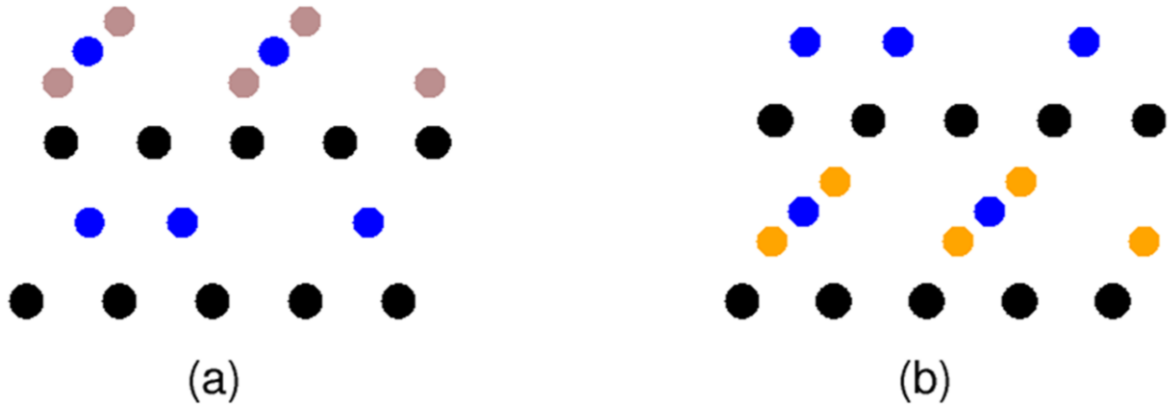

Fig. 7. Schematic illustration of the coupling of atomic arrangements of the terminating metal layer with those at the substrate subsurface layer. (a) A MgAlMg tri-sublayer on the O1-substrate. (b) An Al-layer on O2-substrate. The black spheres represent O, blue Al, orange Mg and the brown for Mg/Al depending on the chemical composition of the liquid (Color figure online).

Ab initio MD simulation provides no accurate interfacial energies for L-Al/$MgAl_2O_4${1 1 1} due to the difficulties in describing of the liquid phase. Here we try to assess the dominant L-Al/$MgAl_2O_4${1 1 1} interface among the investigated ones.

The previous atomistic simulations provided that at ambient conditions, the O atoms form the most stable $MgAl_2O_4${1 1 1} surfaces with an Al2 or a MgAl subsurface layer (surface energies, $\gamma \approx 3.1 J/m^2$) [11]. Furthermore, the Al-terminated surface ($\gamma = 3.46 J/m^2$) is more stable than the MgAl-terminated surface ($\gamma = 2.85$ to $4.09 J/m^2$) [12].

The AIMD simulations revealed that there forms a terminating metallic layer at the L-Al/ $MgAl_2O_4$ {1 1 1} interfaces. From the higher stability of the $MgAl_2O_4$ $\{1\ 1\ 1\}_{Al}$ surface at ambient conditions [12] and the flatness and higher in-plane ordering of the terminating Al2 layer, the L-Al/$MgAl_2O_4$ $\{1\ 1\ 1\}_{Al2}$ interface (Type 2) is considered to be more stable than the Type 1 interfaces.

In heterogeneous nucleation theory, nucleation potency represents the intrinsic capability of a substrate to nucleate a solid phase from the melt. Prenucleation at a liquid/substrate interface relates to the intrinsic capability of the substrate surface to template atomic ordering in the liquid adjacent to the interface, and therefore, corresponds to the potency of the substrate for nucleation of the solid. Recent atomistic investigations revealed three factors affecting prenucleation at a liquid-metal/solid-substrate interface [6]:

- Structural factor: Lattice misfit between metal and substrate (*f*) hinders strongly the in-plane ordering, but affects little on the atomic layering [7, 19].
- Chemical factor: A chemically affinitive substrate promotes atomic ordering at the interface, whereas a repulsive substrate weakens prenucleation [8].
- Atomic roughness: The atomic roughness of a substrate surface (*R*) deteriorates both layering and in-plane ordering at the interface [20].

Our electronic structure calculations and charge analysis provided that the terminating metal atoms at the L-Al/$MgAl_2O_4${1 1 1} interfaces are charged (*q*). We summarize the factors, lattice misfits between the metals and the substrates (*f*), the atomic roughness of the terminating metal layer (*R*), and the charges at the atomic sites (*q*), as well as the related

prenucleation for the L-Al/$MgAl_2O_4${1 1 1} interfaces in Table II. The related results for liquid-Al/solid-Al{1 1 1} [8] are included as reference.

Our previous study on the prenucleation at the L-Al/MgO{1 1 1}$_{Mg}$ interface showed that the terminating Mg layer is well ordered with full occupation. Meanwhile, the Mg atoms are charged ($Mg^{+0.69e}$) [14]. The misfit between solid Al{1 1 1} and MgO{1 1 1} is moderate (-3.8%). However, the prenucleation at the L-Al/MgO{1 1 1}$_{Mg}$ interface is notably weaker than that of the reference (Table II) [8, 14]. Considering that facts the lattice misfit affects little on layering [7, 19] and chemically Mg is affinitive to Al [37], one can conclude that charging hinders prenucleation. The present simulations also showed that charging at the Al/$MgAl_2O_4${1 1 1} interfaces causes the weak prenucleation.

The terminating layer at L-Al/$MgAl_2O_4${1 1 1}$_{Al2}$ is flat but contain atomic vacancies. The small lattice misfit and moderate atomic roughness result moderate prenucleation at L-Al/$MgAl_2O_4${1 1 1}$_{Al2}$. Meanwhile, the pronounced atomic roughness at the Type 1 interfaces weakens prenucleation. Combined study of the interfaces, we list the potency of the substrates to nucleate Al in the series (from high to low): s-Al{1 1 1}$_{Al}$ > $MgAl_2O_4${1 1 1}$_{Al2}$ >> $MgAl_2O_4${1 1 1}$_{MgAlMg}$ ~ $MgAl_2O_4${1 1 1}$_{MgAlAl}$ ~ $MgAl_2O_4${1 1 1}$_{AlAlAl}$.

According to the recent study, there is an energy barrier for grain initiation after heterogeneous nucleation [6]. When temperature is lowered to the grain initiation temperature, grains start to grow freely [6]. Conventionally, people search for potent particles as potential nucleation sites for grain refinement. The successful grain-refiners include the Al-Ti-B master alloys which contain TiB_2{0 0 0 1} substrates [38, 39]. Recently, high-resolution transmission observations revealed that the TiB_2{0 0 0 1} substrates are covered by a two-dimension compound (2DC), most-likely $TiAl_3$ [40]. This 2DC reduces the lattice mismatch between the substrate and Al, enhancing potency of the TiB_2{0 0 0 1}$_{TiAl3}$ substrate to Al [6, 40]. This highly potent substrate requires a small driving force (undercooling) for nucleation of solid Al. In this case, size of the TiB_2 particles plays a crucial role in grain initiation [6, 41]. Heterogeneous nucleation occurs on the particles of all sizes at the same temperature. When the temperature lowers to the grain initiation temperature, grain initiation starts with large particles first and gradually occurs at smaller particles with increasing undercooling. This grain initiation process is considered to be progressive [6], in which only a small number of large-sized particles function as grain-refinement sites.

$MgAl_2O_4${1 1 1} substrates are much less potent to Al than TiB_2{0 0 0 1}$_{TiAl3}$, thus require a larger nucleation undercooling, which might be lower than that of corresponding grain initiation temperature. Under such situation, when temperature reaches the nucleation temperature, the nucleation and grain initiation may occur almost simultaneously, in an explosive way [6]. On most of the substrates could nucleation and grain initiation occur. This means larger fraction of particles become grain-initiation sites. consequently, the solidified alloy may have fine grain sizes, if the spinel particles are of high number density and uniform special distribution in the melt. and no other more potent particles of importance exist in the melt [6].

5. CONCLUSIONS

Using the *ab initio* molecular dynamics simulation, we investigated prenucleation at the L-Al/$MgAl_2O_4${111} interfaces. We revealed the formation of a metal layer that terminates the $MgAl_2O_4${1 1 1} substrates. The newly formed metal layer has a small spacing to the outmost O layer. The atoms at this newly formed layer are chemically charged and structurally

bonded to the outmost O layer of the substrate. The Al atoms/ions at the terminating layer are ordered and behave solid-like. Structurally, the terminating metal atoms at the interfaces are coupled with those of the substrate subsurface layer. The termination Al layer at L-Al/$MgAl_2O_4$$\{1\ 1\ 1\}_{Al2}$ is flat but contains vacancies, whereas the termination Al layers of the rest of the interfaces exhibit out-of-layer displacements. Overall, the ordered terminating layer at the L-Al/$MgAl_2O_4\{1\ 1\ 1\}$ interfaces is atomically rough. The nucleation potency of the substrate for Al has the following order from high to low: L-Al/$MgAl_2O_4$$\{1\ 1\ 1\}_{Al2}$ >> L-Al/$MgAl_2O_4$$\{1\ 1\ 1\}_{MgAlMg}$ ≥ L-Al/$MgAl_2O_4$$\{1\ 1\ 1\}_{MgAlAl}$ ≥ L-Al/$MgAl_2O_4$$\{1\ 1\ 1\}_{AlAlAl}$. The obtained results shed new light on the role of oxide particles in heterogeneous nucleation of Al-Mg alloys.

ACKNOWLEDGEMENTS

Financial support from EPSRC (UK) under grant number EP/N007638/1 is gratefully acknowledged.

REFERENCES

1. H.-T. Li, Y. Wang and Z. Fan: *Acta Mater*. 2012, vol. 60, pp. 1528-1537.

2. K. Kim: *Surf. Interface Anal.* 2015, vol. 47, pp. 429-438.

3. L. Cao, G. C. Wang, Y. Zhao, S. Sridhar and H. Lei: *Metal. Mater. Trans. B* 2019, vol. 50B, pp. 2502-2507.

4. L. Wang, W. Q. Lu, Q. D. Hu, M. X. Xia, Y. Wang and J. Q. Li: *Acta Mater.* 2017, vol. 139, pp. 75-85.

5. Y. J. Zhang, S. H. Wang, E. Lordan, Y. Wang and Z. Fan: *J. Alloys and Compounds* vol. 785, pp. 1015-1022.

6. Z. Fan: Proc. The 11th international conference on magnesium alloys and their applications, 24-27 July 2018, Beaumont Estate, Old Windsor, UK. Ed. By Z. Fan and C. Mendis, 2018, pp. 7-17.

7. H. Men and Z. Fan: *Metall. Mater. Trans. A* 2018, vol. 49A, pp. 2766-2777.

8. C. M. Fang, H. Men and Z. Fan: *Metall. Mater. Trans. A* 2018, vol. 49A, pp. 6231-4242.

9. Z. Fan: *Metal. Mater. Trans. A*, 2013, vol. 44A, pp. 1409-1418.

10. K. E. Sickafus, J. W. Wills and N. W. Grimes: *J. Am. Ceram. Soc.* 1999, vol. 82, pp. 3279-3292.

11. C. M. Fang, S. C. Parker and G. de With: *J. Am. Ceramic Soc*. 2000, vol. 83, pp. 2082-2084.

12. M. J. Davies, S. C. Parker and G. W. Watson: *J. Mater. Chem*. 1994, vol. 4, pp. 813-816.

13. C. M. Fang and Z. Fan: *Comp. Mater. Sci*. 2020, vol. 171, p. 109258.

14. C. M. Fang and Z. Fan: *Philos. Mag. Lett.* 2020, vol. 100, pp.235-244

15. G. Singh, Y. Yu, F. Ernst and R. Raj: *Acta Mater.* 2007, vol. 55, pp. 3049-3057.

16. P. Shen, H. Fuji, T. Matsumoto and K. Nogi: *Acta Mater*. 2004, vol. 52, pp. 887-989.

17. A. Hashibon, J. Adler, M. W. Finnis and W. D. Kaplan: *Comp. Mater. Sci*. 2002, vol. 24, pp. 443-452.

18. W. D. Kaplan and Y. Kauffman: *Ann. Rev. Mater. Res.* 2006, vol. 36, pp. 1-48.

19. H. Men and Z. Fan: *Comp. Mater. Sci*. 2014, vol. 85, pp. 1-7.

20. B. Jiang, H. Men and Z. Fan: *Comp. Mater. Sci*. 2018, vol. 153, pp. 73-81.

21. R. Scheinfest, S. Kostlmeier, F. Ernst, C. Elsasser, T. Wagner and M. W. Finnis: *Philos. Mag. A* 2001, vol. 81A, pp. 927-955.

22. J. S. Wang, A. P. Horsfield, U. Schwingenschlögl and P. D. Lee: *Phys. Rev. B* 2010, vol. 82B, p. 144203.

23. D. Wearing, A. P. Horsfielf, W. W. Xu, and P. D. Lee: *J. Alloys and Compounds* 2016, vol. 664, pp. 460-468.

24. Y. Kauffmann, S. H. Oh, C. T. Koch, A. Hashibon, C. Scheu, M. Rühle and W. D. Kaplan: *Acta Mater*. 2011, vol. 59, pp. 4378-4386.

25. S. D. Ma, A. J. Brown, R. Yan, R.L. Davidchack, P. B. Howes, C. Nicklin, Q. J. Zhai, T. Jing and H. B. Dong: *Commun. Chem*. 2019, vol. 2, p. 1.

26. C. M. Fang and Z. Fan: *Metall. Mater. Transaction A* 2020, vol. 51, pp. 788-797.

27. J.W. Arblaster: *Selected values of the crystallographic properties of the elements*, ASM International, Materials Park, Ohio, 2018, pp. 124-132.

28. G. Fiquet, P. Richet and G. Montagnac: *Phys. Chem. Miner*. 1999, vol. 27, pp. 103-111.

29. G. Kresse and J. Hafner: *Phys. Rev. B* 1994, vol. 49B, pp. 14251-14269.

30. P. E. Blöchl: *Phys. Rev. B* 1994, vol. 50B, pp. 17953-17978.

31. J. P. Perdew and K. Burke, M. Ernzerhof: *Phys. Rev. Lett.* 1996, vol. 77, pp. 3865-3868.

32. H. J. Monkhorst and J. D. Pack: *Phys. Rev. B* 1976, vol. 13B, pp. 5188-5192.

33. D. G. Sangiovanni, G. K. Gueorguiev and A. Kakanakova-Georgieva, *Phys. Chem. Chem. Phys.* 2018, vol. 20, pp. 17751-17761.

34. R. F. W. Bader: *J. Phys. Chem. A* 1998, vol. 102A, pp. 7314-7323.

35. G. Henkelman, A. Arnaldsson and H. Jónsson: *Comp. Mater. Sci*. 2006, vol. 36, pp. 354-360.

36. I. D. Brown: *Chem. Rev.* 2009, vol. 109, pp. 6858–6919.

37. A. Takeuchi and A. Inoue: *Mater. Trans*. 2005, vol. 46, pp. 2817-2829.

38. A. Cibula: *J. Inst. Met.* 1951, vol. 80, pp. 1-16.

39. A. L. Greer, A. M. Bunn, A. Tronche, P.V. Evans and D. J. Bristo: *Acta Mater*. 2000, vol. 48, pp. 2823-2835.

40. Z. Fan, Y. Wang, Y. Zhang, T. Qin, X. R. Zhou, G. E. Thompson and T. Hashimoto: *Acta Mater*. 2015, vol. 84, pp. 292-304.

41. K.F. Kelton, A.L. Greer: *Nucleation in condensed matter: applications in materials and biology*, Pergamon Materials Series, Elsevier Ltd. Oxford/Amsterdam, 2010, pp. 181-204, pp. 473-478.

Legends for Figures

Fig.1. Schematic structure of $MgAl_2O_4$ in the hexagonal cell (a) and atomic arrangements of the related O1- (b), O2- (c), Al2- (d), Mg- sublayer (e) and MgAl- double-sublayers (f) and MgAlMg- tri-sublayers (g) terminating the spinel{1 1 1} substrates. The orange spheres represent Mg, silvery Al and dark blue O. The reddish lines represent the unit cell axis (Color figure online).

Fig. 2. Snapshots for the evolutions of the L-Al/$MgAl_2O_4${1 1 1}$_{O1}$ (a), L-Al/$MgAl_2O_4${1 1 1}$_{Mg}$ (b) and L-Al/$MgAl_2O_4${1 1 1}$_{MgAlMg}$ (c) and L-Al/$MgAl_2O_4${1 1 1}$_{O2}$ (d) interfaces (Table I) at the beginning of the *ab initio* molecular dynamics simulations (the second and third columns) and the equilibrated configurations (the last column) at 1000K. The orange spheres represent Mg, silvery Al and dark blue O (Color figure online).

Fig. 3. Atomic density profiles at a) L-Al/$MgAl_2O_4${1 1 1}$_{MgAlMg}$, b) L-Al/$MgAl_2O_4${1 1 1}$_{MgAlAl}$, c) L-Al/$MgAl_2O_4${1 1 1}$_{AlAlAl}$, and d) L-Al/$MgAl_2O_4${1 1 1}$_{Al2}$. The dotted line (at x = 0) represents the plane of the terminating metal layer and the broken lines represent the 1st to 4th Al layer.

Fig. 4. Snapshots of the layer-resolved atomic arrangements at the L-Al/$MgAl_2O_4${1 1 1}$_{AlAlAl}$ (a), L-Al/$MgAl_2O_4${1 1 1}$_{MgAlAl}$ (b), L-Al/$MgAl_2O_4${1 1 1}$_{MgAlMg}$ (c), and L-Al/$MgAl_2O_4${1 1 1}$_{Al2}$ (d) interfaces. The reddish lines represent in-plane axis. The silvery spheres represent Al and the orange for Mg (Color figure online).

Fig. 5. In-plane ordering coefficients of the atomic layers near the L-Al/$MgAl_2O_4${1 1 1} interfaces. The number in the x-axis: 0 represents the terminating metal-layer, n the nth Al-layer (Color figure online).

Fig. 6. Charges at the atomic sites at the L-Al/$MgAl_2O_4${1 1 1} interfaces. The black spheres represent charges at Al, orange at Mg and blue at O. (Color figure online).

Fig. 7. Schematic illustration of the coupling of atomic arrangements of the terminating metal layer with those at the substrate subsurface layer. (a) A MgAlMg tri-sublayer on the O1-substrate. (b) An Al-layer on O2-substrate. The black spheres represent O, blue Al, orange Mg and the brown for Mg/Al depending on the chemical composition of the liquid (Color figure online).